Nuclear Instruments and Methods in Physics Research A 594 (2008) 232–243

Contents lists available at ScienceDirect

Nuclear Instruments and Methods in Physics Research A

journal homepage: www.elsevier.com/locate/nima

Energy calibration of gamma spectra in plastic scintillators using Compton kinematics

E.R. Siciliano, J.H. Ely, R.T. Kouzes *, J.E. Schweppe, D.M. Strachan, S.T. Yokuda

Pacific Northwest National Laboratory, MS K7-36, National Security Division, 1005 Country Court, P. O. Box 999, Richland, WA 99352, USA

ARTICLE INFO

Article history:
Received 20 January 2008
Accepted 24 June 2008
Available online 1 July 2008

Keywords:
Gamma-ray detection
Portal monitor
Radiation detection
Homeland security
Border security
Detection of illicit materials
Monte Carlo modeling
Detector calibration

ABSTRACT

This paper describes a simple and practicable method for assigning energy values to gamma-ray pulse-height distributions measured with polyvinyl toluene (PVT) based detectors. It is based upon the characteristic shape of simulated spectra in the region of maximum energy deposition resulting from a single Compton scattering. The validity of this method is demonstrated by applying it to a set of measured NaI(Tl) spectra, and comparing those results to the standard photopeak method of calibrating the same spectra. The method is then applied to a set of measured PVT spectra. It can now be applied to calibration of fielded PVT detectors using two selected gamma-ray sources, which was the initial motivation for this study.

1. Introduction

The ability to associate gamma-ray energy values to regions of measured pulse-height spectra from radiation detectors requires the presence of discernable and physically well-understood structures in spectra. The simplest situation is for those scintillating materials where photon interactions can occur primarily by the photoelectric absorption mechanism. For such detectors, full-energy peaks are easily observed and are well localized, allowing their centroids to be assigned specific energy values without further analysis or model dependence. If over this same energy region a scintillation material is used in which gamma rays are much more likely to interact by single Compton scattering than by photoabsorption, full-energy peaks are not observed, and energy calibration of the corresponding pulse-height spectra is more challenging. For sources whose highest-energy gamma rays are well isolated and dominant, spectra in such materials can show a discernable structure in the region that corresponds to the maximum energy deposited by a single Compton scattering—the Compton edge (CE). Unlike full-energy photoabsorption peaks, the maximum of the CE structure is broad and asymmetrical. Thus, deciding which region of this structure is assigned to the CE energy value requires some analysis. This paper describes such an analysis and prescribes a simple and easily applied method for assigning CE energy values to Compton maxima regions of polyvinyl toluene (PVT)-based detector spectra.

One practical need for energy calibration of PVT-based detectors derives from their increased use in radiation portal monitors (RPMs) installed at all major US land border crossings and seaports to intercept illicit radioactive materials [1,2]. Routine procedures are used to test and calibrate these systems, and the ability to relate energy values to measured channels is important to their continued correct operation [3]. As described by Ely et al., one particular need for such energy calibration in PVT-based RPMs is the use of "Energy Windowing" algorithms. Even though the energy information from these detectors is limited to broad Compton structures, Energy Windowing algorithms are able to use such information to discriminate between certain types of materials based upon subtle differences in spectra over a few (~8), relatively wide regions of interest. Count rates in these regions are manipulated algorithmically to provide discrimination based upon the energy spectrum of the source. The development of the method described in this paper was motivated by, and directed towards, such RPM applications in terms of the energy range of interest and its ease of use in the field. Although the intrinsic energy "resolution" of PVT is poor, the precision required for determining the window boundaries in such RPM applications can be obtained with the method described here.

Before outlining the method, it is worth pointing out some of the factors that affect the observed spectral shape seen with

* Corresponding author. Tel.: +1 509 372 4858; fax: +1 509 372 4969.
E-mail addresses: richard.kouzes@pnl.gov, rkouzes@pnl.gov (R.T. Kouzes).

0168-9002/$ - see front matter © 2008 Published by Elsevier B.V.
doi:10.1016/j.nima.2008.06.031

PVT-based detectors, for which there are at least four factors: (1) the underlying Compton nature of the energy loss mechanism, (2) the non-linear physics of the scintillation process that converts deposited energy to light, (3) the geometry-dependent low percentage of light collected from the detector, and (4) the variation in light collection from different positions across a large detector. It is not the intent of this paper to explain these physics mechanisms, but rather simply to show a consistent and easy to use method for energy calibration of PVT. The approach used successfully combines these effects together to match the empirically observed spectra using a single model parameter.

The key element in the calibration method presented below is the "ratio algorithm" for relating the position of the broad Compton maximum (CM) to the corresponding CE energy value, since the CM is more easily located in spectra. The determination of this algorithm was based upon Monte Carlo calculations of simulated photon response distributions suitable for comparison to those observed in measured spectra. These simulations were performed with the Monte Carlo n-particle (MCNP) code [4] for a simple model of a detector in which the correlation between the CM and its CE could be studied for a variety of effects. This modeled correlation was then applied to experimental data. The concept is first validated using thallium-doped sodium iodide [NaI(Tl)] scintillator spectra in which both full-energy peaks and CE structures are observed. Following this validation, it was then applied to PVT-based scintillators. Application of this technique with several gamma-emitting radioisotopes under controlled conditions is demonstrated.

There have been many articles written on the application of MCNP calculations to simulate the spectra resulting from photon interactions in various detector materials such as NaI(Tl), Si, Ge, and HPGe (e.g., see Refs. [5–10]). Because the most important physical processes have been taken into account in these simulations, results have shown very good agreement with experimental data. Many studies of organic (solid or liquid) scintillators, such as PVT, reported to date involve the use of MCNP calculations for the response of these materials to neutrons. Normand et al. [11] used MCNP in combination with two other codes to calculate the spectrum from a boron-loaded plastic scintillator. Other articles on the response of scintillator materials to neutrons and gamma rays have been published, including Refs. [12–24]. Simulations of spectra resulting from photon interactions for a variety of sources with NaI(Tl) and PVT-based gamma-ray detectors have been reported by Siciliano et al. [25]. In all of the above references, however, no study had the goal of energy-calibrating detectors made from organic scintillator materials.

2. Analysis framework

The analysis described in this paper was focused upon homeland security applications, where the gamma-ray energies

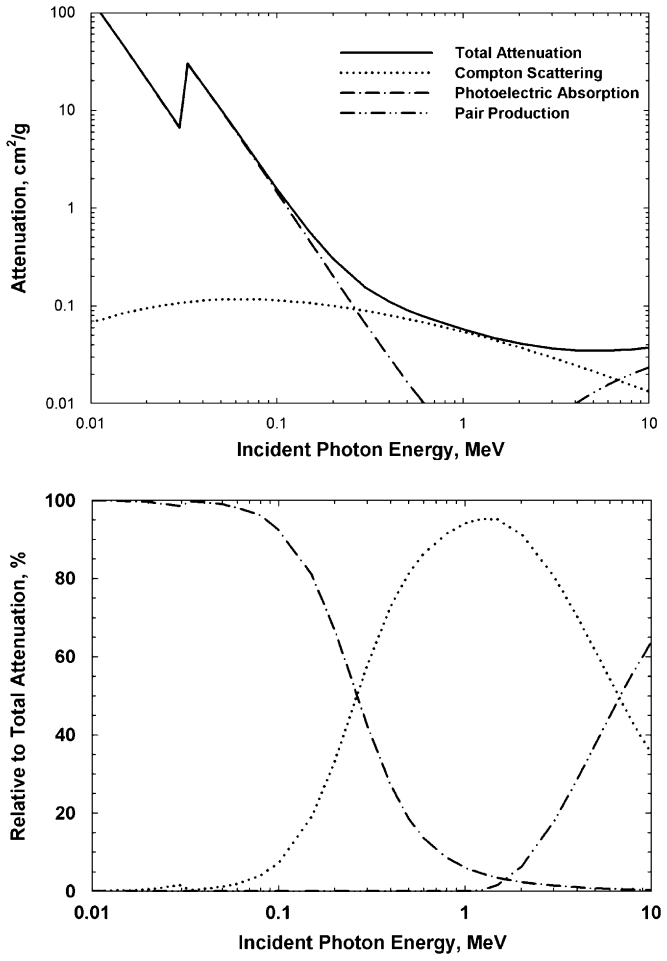

Fig. 1. Absolute (upper graph) and relative (lower graph) comparison of photon interactions in NaI(Tl).

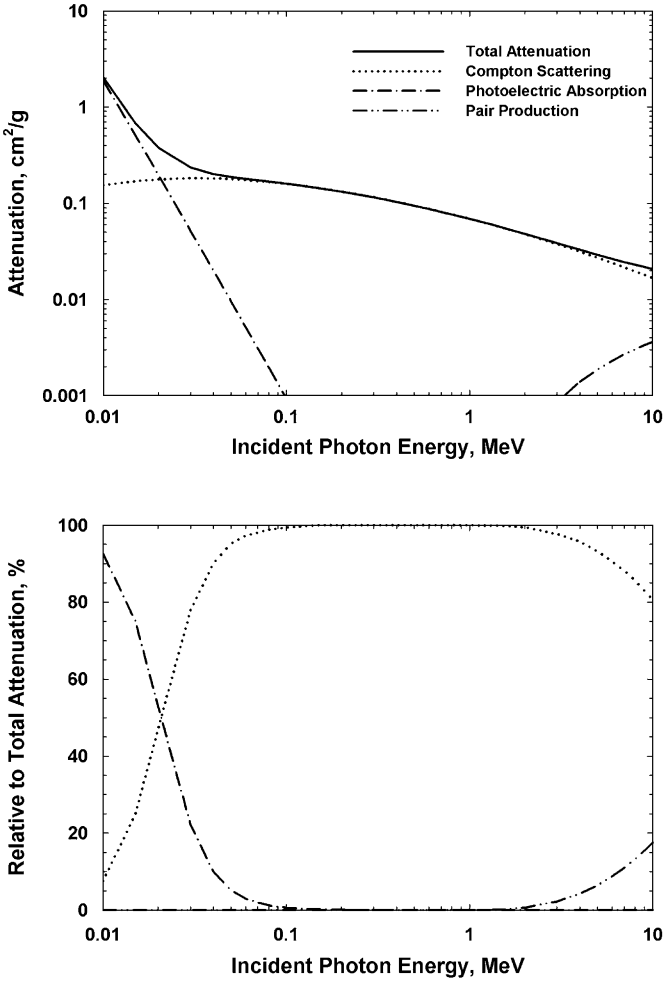

Fig. 2. Absolute (upper graph) and relative (lower graph) comparison of photon interactions in PVT.

of interest are primarily in the range of 0–3000 keV. In this energy range, the primary interaction mechanism for gamma rays in PVT is single Compton scattering events, whereas photoelectric absorption and multiple Compton scattering are significant for NaI(Tl) scintillators. It is instructive to look at the comparison between these two scintillator materials for photons of varying energies. The XCOM program [26] can be used to show the contribution to photon attenuation from the photoelectric effect, Compton scattering, and electron–positron pair production for NaI(Tl) and PVT (input as vinyl toluene, $CH_3C_6H_4CH{=}CH_2$). The results are shown in Figs. 1 and 2, respectively, where the upper graphs show the absolute contribution to the total photon attenuations and the lower graphs show the relative contributions from each of these effects to the total attenuation. From Fig. 1, it can be seen that in NaI(Tl) the photon interactions are characterized by the photoelectric absorption for energies up to about 0.3 MeV, above which Compton scattering dominates to a few MeV. For PVT scintillator (Fig. 2), however, Compton scattering dominates over most of the operating range of interest. Only at very low energies does the photoelectric effect become important for PVT-based detectors, amounting to about 50% of the interaction at 20 keV. In both cases, the effects of pair production do not contribute significantly (~5% at 2 MeV for NaI) over the operating range of interest.

Because of the low atomic number of the constituents of PVT and the relatively long gamma-ray interaction length, gamma rays usually Compton scatter only once before exiting the typical detector and rarely undergo photoelectric absorption. The inherently poor photopeak resolution of typical large PVT-based detectors, combined with the low probability of photoelectric events results in no full-energy peaks being visible in the pulse-height distribution for energies of interest. As mentioned above, this makes calibration of the pulse-height distribution (to convert to an energy distribution) much more challenging for PVT than for spectroscopic quality scintillation materials such as NaI(Tl) crystals.

The goal of this work was to show that energy calibration of PVT can indeed be accomplished by using the CE values for known sources. Because multiple scattering events tend to broaden the PVT response function in the region of the CE by extending the distribution to higher energies, the goal was to develop a reliable algorithm for deciding where in the pulse-height distribution the CE value occurs.

To determine the relationship between the maximum in the CE region of the response functions and the position of the CE energy, a series of simple MCNP model calculations were performed. These calculations were carried out using the full-energy spectra from five radionuclides that emit gamma photons in the range from about 100 to about 3 MeV. Model pulse-height distributions for PVT and NaI(Tl) were obtained for these sources, and ratios of the pulse-height count values at the CM to their values at the corresponding CE energies were tabulated. By using the Gaussian energy-broadening feature of MCNP, it was possible to study how different "intrinsic resolution values" affected the behavior of the CE regions and their effects on the CE-to-CM ratios.

To test the validity of prescription embodied by the simulated CE-to-CM ratios, pulse-height distributions measured by an NaI(Tl) detector were calibrated with two methods: the traditional

Table 1
Photon emission data for model sources used in MCNP simulations

Isotope	Emitted photon energies (keV) and percent branching fractions (%BF)[a]									
^{133}Ba										
Energy	3.79	4.14	4.28	4.73	5.39	*30.63*	*30.97*	*34.97*	*36.01*	53.15
%BF	0.24	0.11	6.70	6.52	0.91	*35.56*	*65.74*	*17.97*	*4.40*	2.17
Energy	*79.61*	*80.99*	160.60	223.24	*276.39*	*302.85*	*356.00*	**383.84**		
%BF	*3.18*	*34.18*	0.60	0.46	*7.09*	*18.40*	*62.15*	**8.92**		
^{57}Co										
Energy	0.62	0.63	0.70	0.73	*6.39*	*6.4*	7.06	7.17	14.41	*122.06*
%BF	0.07	0.05	0.65	0.50	*16.41*	*32.5*	5.84	–	9.54	*85.54*
Energy	**136.47**	230.26	339.66	352.32	366.74	569.92	691.98	706.39		
%BF	**10.69**	–	–	–	–	–	0.16	–		
^{60}Co										
Energy	346.95	826.33	**1173.2**	**1332.5**	2158.9	2505.7				
%BF	–	–	**99.90**	**99.98**	–	–				
^{137}Cs										
Energy	3.95	4.33	4.46	4.94	5.62	31.82	32.19	36.36	37.45	**661.66**
%BF	–	–	0.40	0.37	–	2.05	3.77	1.04	0.26	**85.21**
^{232}Th										
Energy	10.26	10.83	11.12	12.28	12.33	12.76	12.95	13.10	*13.52*	15.15
γ/(s g)[b]	118	256	35.1	138	122	750	596	235	*3950*	395
Energy	15.23	15.38	16.15	*16.18*	17.95	18.80	19.11	19.40	39.85	74.81
γ/(s g)	184	41.2	808	*1780*	41.4	513	183	35.5	42.8	411
Energy	74.97	77.11	84.26	87.19	89.96	90.13	93.35	99.55	105.36	129.04
γ/(s g)	50.3	691	47.1	244	135	72.5	220	52.9	79.5	116
Energy	153.89	209.39	*238.58*	240.76	270.26	277.28	300.03	328.07	338.42	409.63
γ/(s g)	33.31	163	*1700*	152	149	95	130	137	491	86.9
Energy	463.11	510.61	562.65	581.53	*583.02*	677.07	726.63	727.25	755.28	772.28
γ/(s g)	180	302	39.9	59.4	*1200*	33.8	34.4	259	52.1	43.0
Energy	785.51	794.79	835.60	840.44	860.30	904.29	*911.16*	964.64	968.97	1459.2
γ/(s g)	43.1	181	67.5	37.1	168	35.2	*1140*	228	688	41.8
Energy	1496.0	1588.2	1620.7	1630.5	**2614.4**					
γ/(s g)	41.5	142	58.8	77.0	**1400**					

[a] Only shown for BF > 0.1%.
[b] Gammas per (s g).

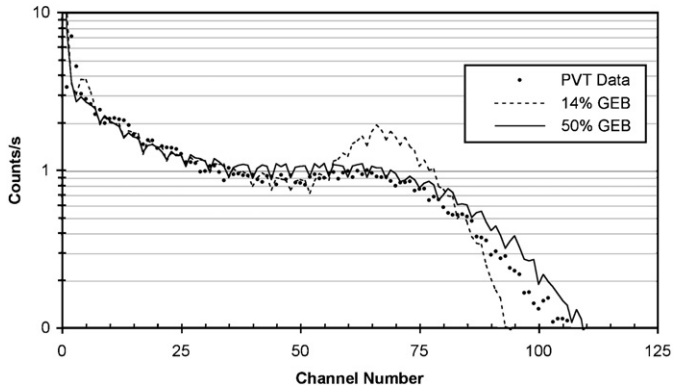

Fig. 3. Comparison of experimental data for a ^{137}Cs source from a PVT-based detector and results from the MCNP detector model for GEB values of 14% and 50% (“Normal” PVT).

method with the full-energy peaks and then with the new CE-to-CM ratio algorithm described here. Good agreement, as discussed below, was obtained between the two calibration methods assuming a linear relationship for NaI(Tl) (which is an approximation) and encouraged the extension of the Compton calibration method to PVT. The same data fitting process was then applied to the PVT, where a different set of Compton-maxima parameters were used to match experimental data. These fits were then used to calibrate the measured PVT data set for the same set of gamma-ray sources.

3. Sources

For simulations performed here, 1 cm diameter uniform spherical sources of ^{133}Ba, ^{57}Co, ^{60}Co, ^{137}Cs and ^{232}Th were used in the MCNP model. These radionuclides were selected because

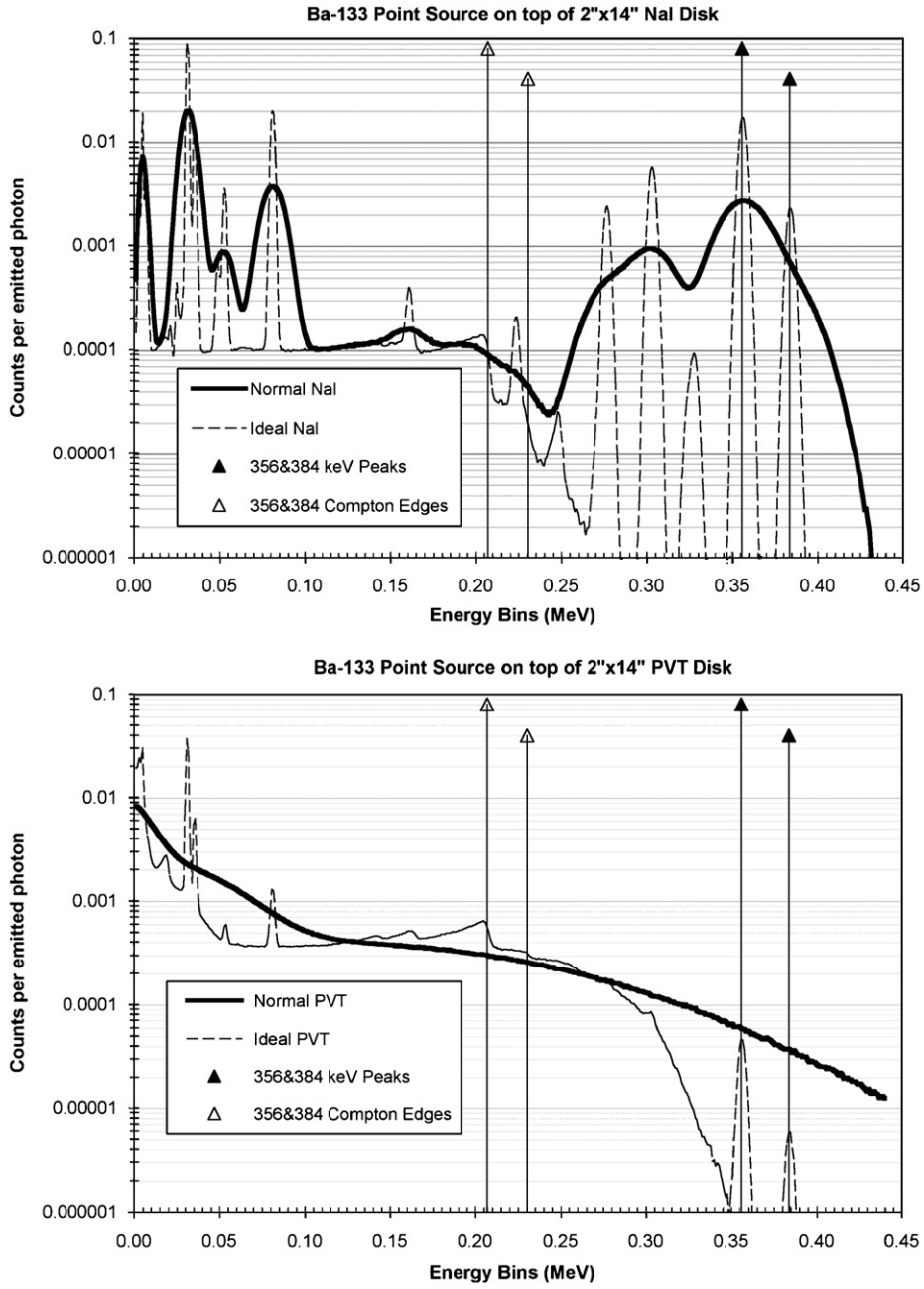

Fig. 4. Computed photon pulse-height efficiency for ^{133}Ba in NaI(Tl) and PVT scintillators.

they each have a dominant high-energy gamma-ray emission that, except for ^{133}Ba and ^{60}Co, is well separated from lower-energy emissions. The values of the high-energy gamma rays from these isotopes span the full-energy range of interest from ~100 to ~2.7 MeV (Table 1).

Table 1 lists the emission energies and percent branching fractions (%BF) or, in the case of ^{232}Th, emission rate per gram used in the model for the five radionuclides [27]. Table entries for the dominant highest-energy gamma ray emitted from each isotope are bold; other gamma rays of comparable strength are italics. Except for ^{133}Ba, ^{57}Co and ^{60}Co, all of the comparable gamma-ray energies are separated from the dominant highest-energy gamma ray by more than 150 keV. Compared to ^{232}Th, the other isotopes have simpler spectra. Out of the 363 tabulated lines for ^{232}Th, the most prevalent 65 were used that account for more than 95% of the total number of gamma-ray emissions per gram.

4. Compton kinematics

Gamma-ray photons that enter a detector sometimes interact by means of the Compton scattering mechanism. In such interactions, the energy (E_1) of the scattered photons is given by the Compton kinematics equation:

$$E_1 = E_0 \frac{m_e c^2}{m_e c^2 + E_0(1 - \cos\theta)} \quad (1)$$

where E_0 is the initial photon energy, m_e is the rest mass of the electron, c the speed of light, and θ is the angle between the incoming and scattered photon. The maximum energy loss of the photon corresponds to the CE energy in the detector response and is obtained when the scattering angle is a maximum at 180°, and thus E_1 is a minimum. The energy deposited is then $E_0 - E_1$.

To calculate CE energy that corresponds to each of the dominant, highest-energy emissions for each radioisotope shown

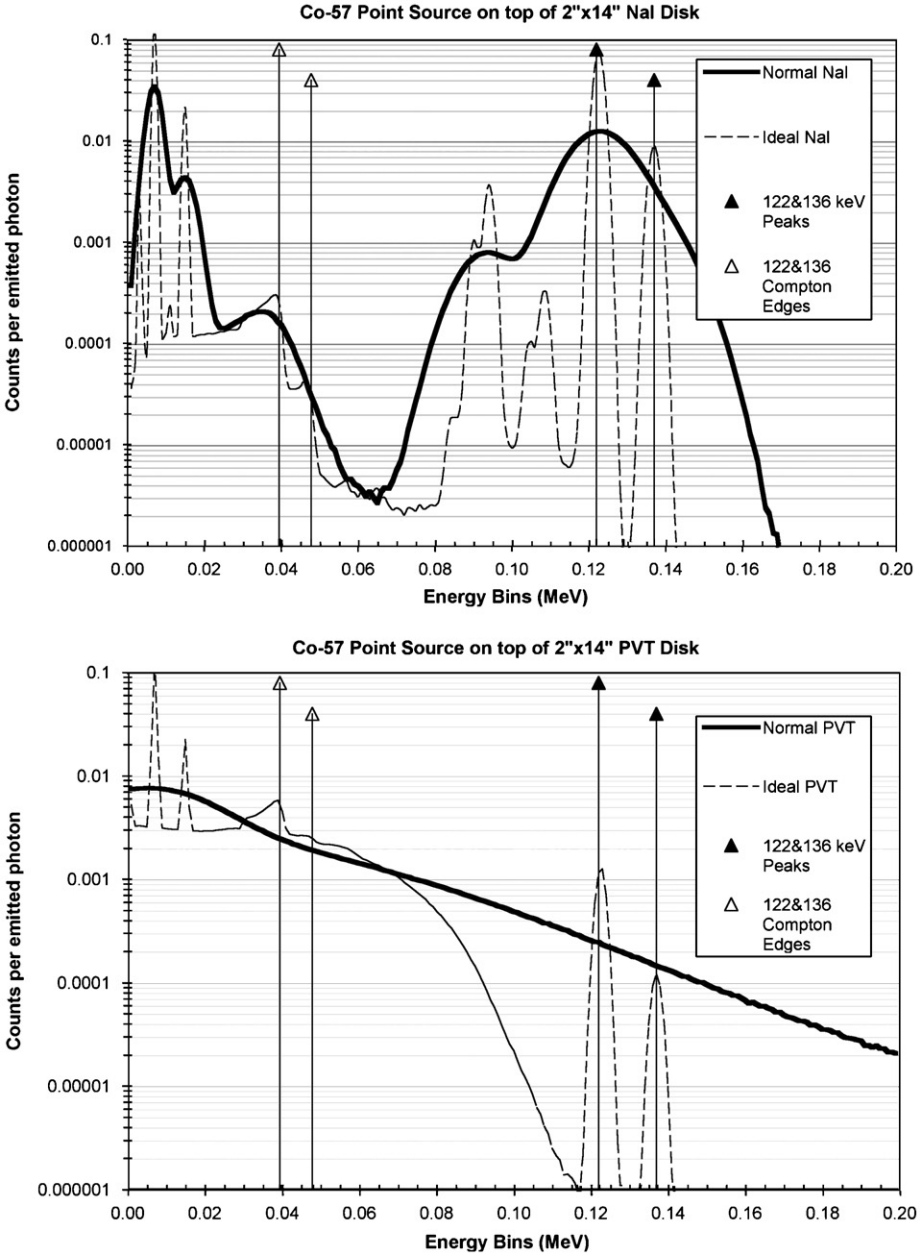

Fig. 5. Computed photon pulse-height efficiency for ^{57}Co in NaI(Tl) and PVT scintillators.

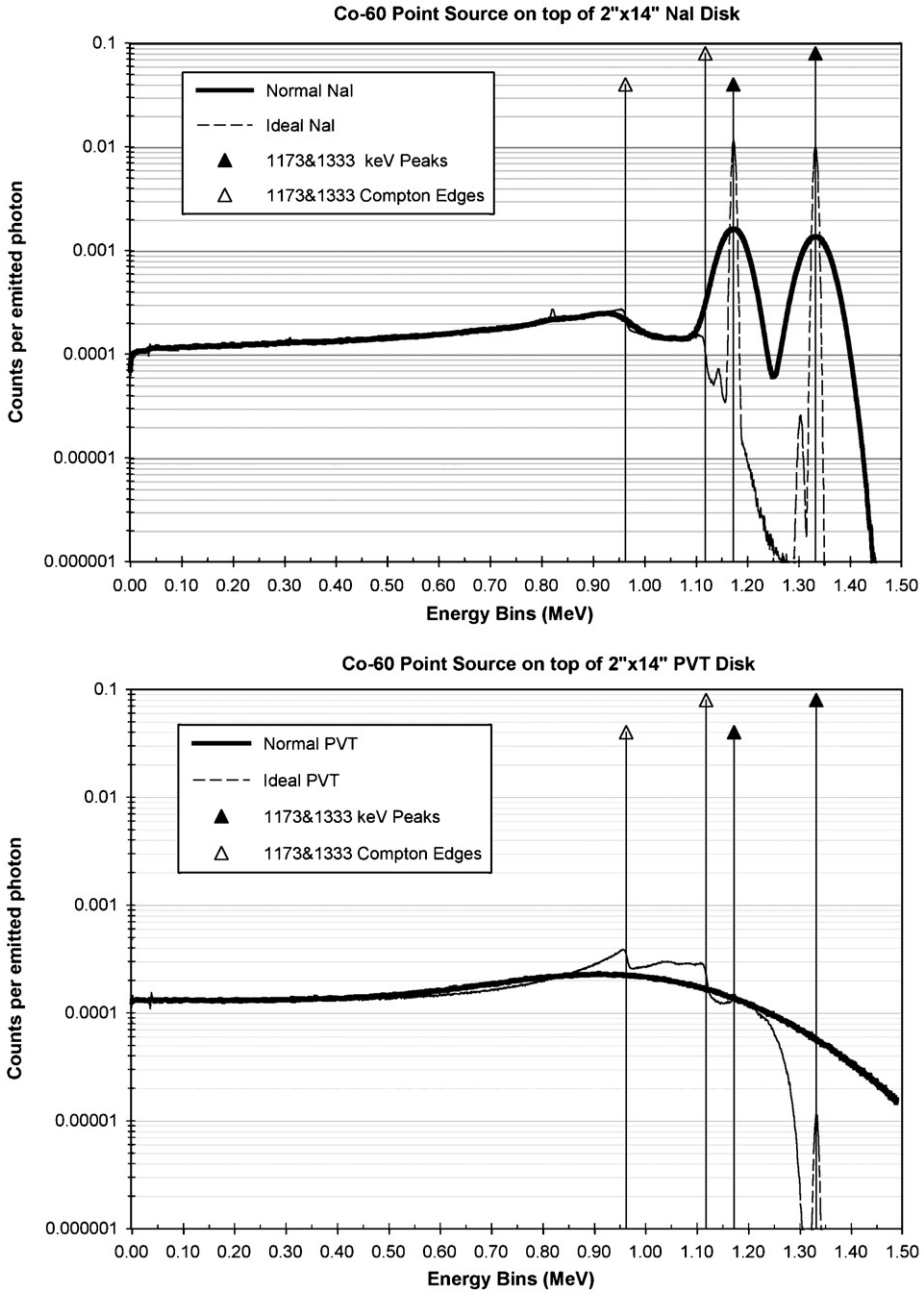

Fig. 6. Computed photon pulse-height efficiency for ^{60}Co in NaI(Tl) and PVT scintillators.

in Table 1, the Compton scattering formula at the maximum scattering angle was used to obtain

$$\text{Edge} = E_\gamma\left(\frac{2E_\gamma}{m_e c^2 + 2E_\gamma}\right) \quad (2)$$

where E_γ is the incident photon energy and $m_e c^2$ is the electron rest energy (511 keV).

5. Model detector calculations

The geometry of the modeled detector was selected to be a right circular cylinder of thickness 5 cm (2″) and diameter 36 cm (14″), and the source center was placed just above the center of one of the circular faces. Cases were evaluated for both NaI(Tl) and PVT comprising the detector material. This geometry is of the scale of typical detectors, and was chosen for simplicity in modeling. The exact geometry of the detector was of little consequence to this study since light collection, or any other specific mechanism for shape broadening, was not evaluated separately. Instead, for each case the energy broadening of the spectra, as specified by the Gaussian Energy Broadening (GEB) option[1] in MCNP, was varied to eliminate the effect of energy

[1] The GEB option in MCNP is used to better simulate a physical detector by sampling from a Gaussian distribution the calculated energy deposited. This option is used to approximate all the resolution effects of detectors that produce broadened spectral features from delta function input energies. Its use produces spectra that very closely match measured spectra from physical detectors, and thus is necessary for the comparison of MCNP calculated spectra with actual spectra.

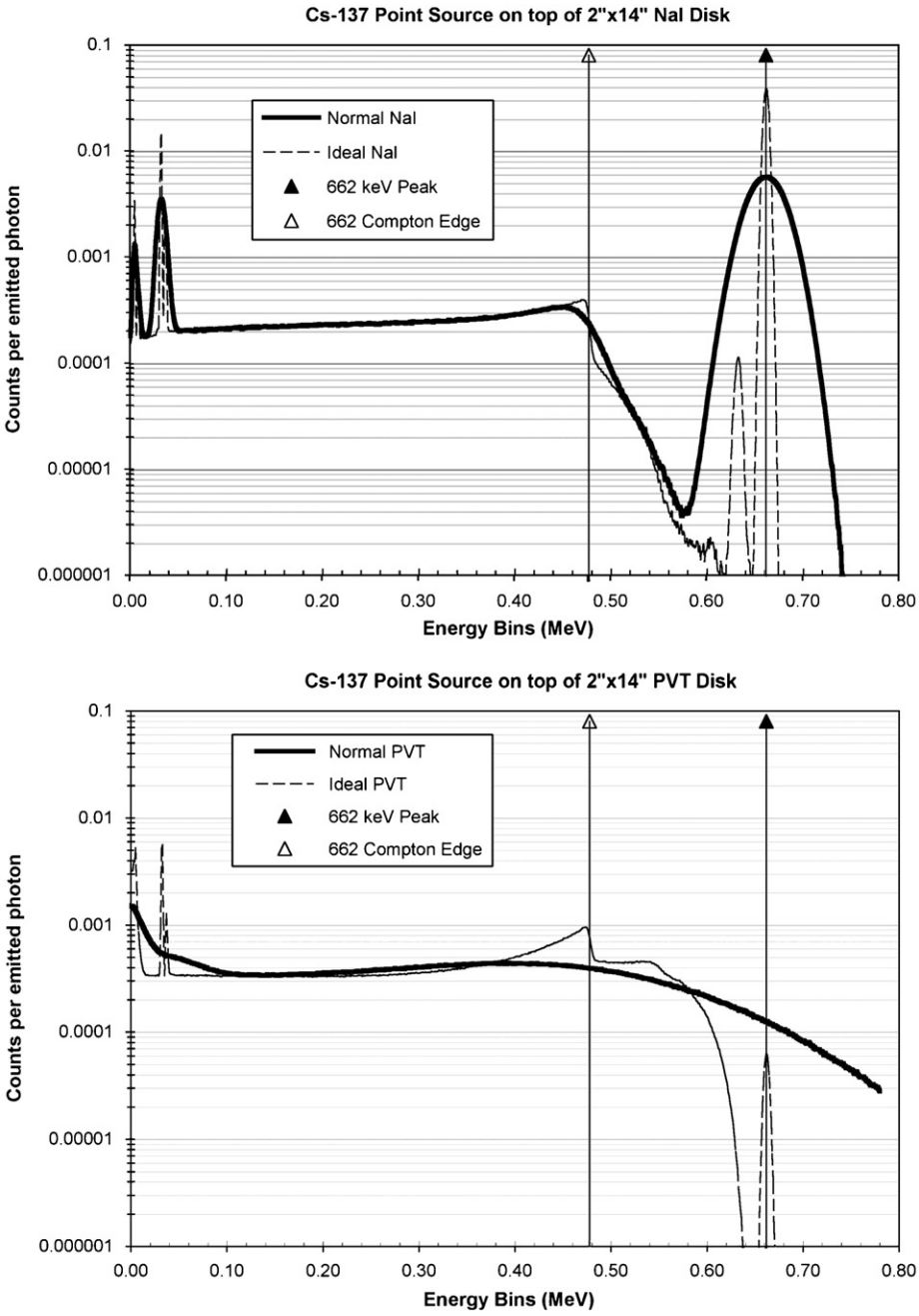

Fig. 7. Computed photon pulse-height efficiency for ^{137}Cs in NaI(Tl) and PVT scintillators.

broadening from the responses. This GEB option in MCNP is used to approximate peak-broadening seen in detectors and is implemented through the formula for peak full-width at half-maximum:

$$\mathrm{FWHM}(E) = a + b\sqrt{(E + cE^2)} \tag{3}$$

where the parameters (a, b, c) used in these simulations had values (0.0, 0.05086, 0.30486) for "normal" NaI(Tl) and (0.0, 0.407, 0.0) for "normal" PVT. These values give a percent FWHM(E) to E ratio at $E = 0.662$ MeV of approximately 7% for NaI(Tl), which is typical for this detector material. For NaI(Tl), the resulting spectra are comparable in appearance to those obtained experimentally. Although the value of the GEB parameter for PVT does not significantly affect the results of the ratio method below, a value of 50% provided the best fit to the experimental data.[2] For part of this study and for each radionuclide modeled, these parameters were varied from the "best-fit" values to smaller values corresponding to about 1% energy broadening[3] to show the intrinsic Compton scattering physics without the broadening effects. No other renormalization of the MCNP output was implemented, i.e., no attempt was made to account for any light-collection

[2] Models for PVT were evaluated for GEB parameters of 1%, 14%, 25%, 50% and 75%.

[3] While no GEB could have been used, 1% GEB is small compared to the actual resolution of these detectors, but provides spectra that are visually easy to analyze.

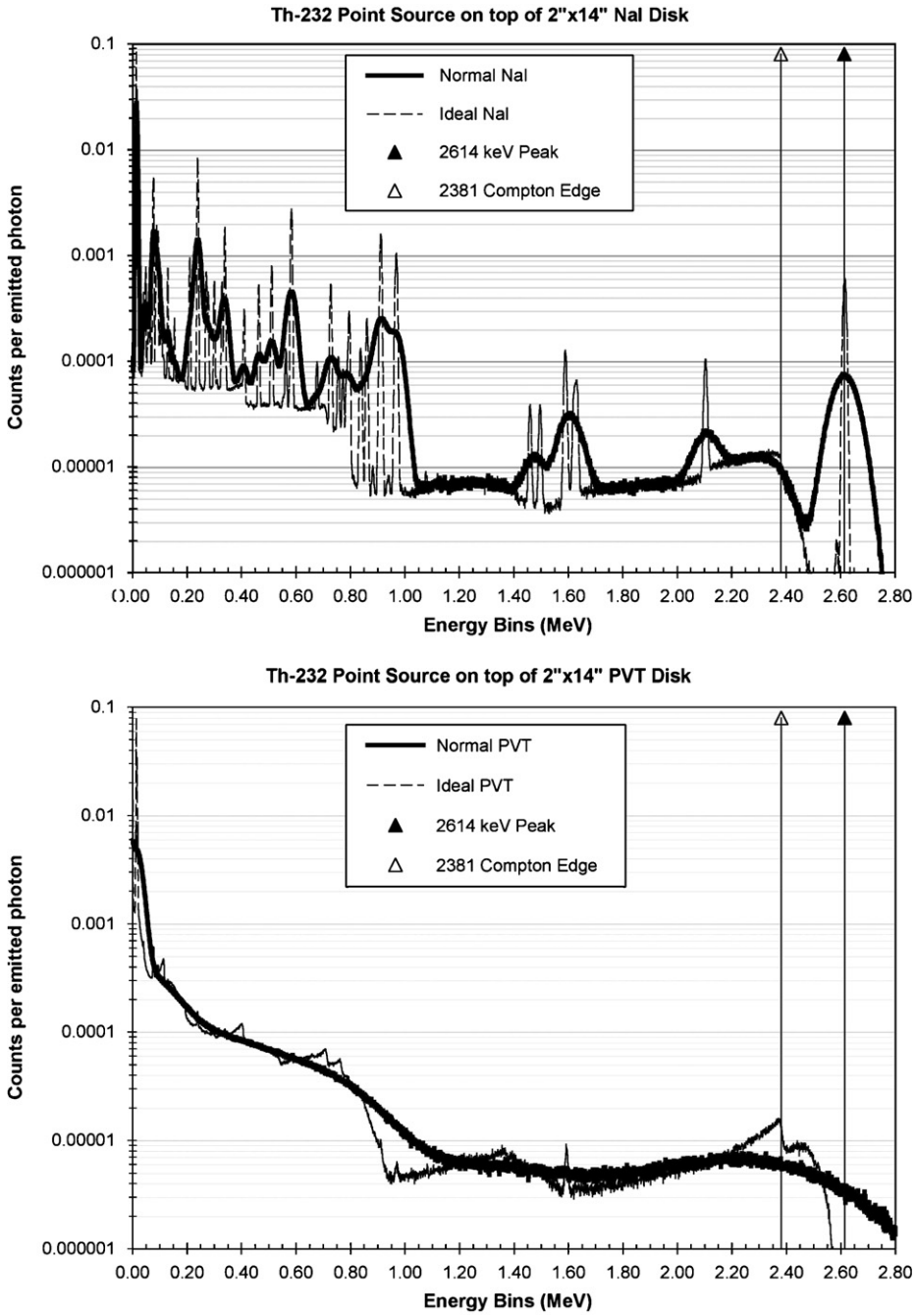

Fig. 8. Computed photon pulse-height efficiency for ^{232}Th in NaI(Tl) and PVT scintillators.

inefficiency within the detector[4]. All calculations were checked for statistical convergence by satisfying the internal statistical checks in MCNP that are used to form confidence intervals for the mean for each tally bin; most results have statistical uncertainties $<1\%$.

Fig. 3 shows a comparison of experimental data for a ^{137}Cs source from a PVT-based detector and results from the MCNP detector model for GEB values of 14% and 50%. The model with a GEB value of 14% looks very different from the data, while the 50% GEB model looks very similar to the experimental data in shape. This good match between empirical data and the MCNP model using GEB to lump together all the effects that generate the observed broad PVT spectra is taken as validation of the approach used. The channel number at which the CM occurs in the three curves shown in Fig. 3 are 61, 66, and 55 for the data, 14% and 50% GEB curves, respectively. This 11-channel shift between 14% and 50% GEB shows the relative sensitivity of the CM fit for PVT to the model GEB parameter. The model with 50% GEB was used for all analysis of the PVT data described in this paper.

Figs. 4–8 show the results of the MCNP model calculations of the energy spectra of five radionuclides for both NaI(Tl) (upper graphs) and PVT (lower graphs). In each of these graphs, the positions of the highest-energy gamma-ray energies from the

[4] Other model-to-measurement validation studies have shown that the MCNP model spectra tend to overestimate measured intensity by an approximately constant factor of 20–30% in the energy range of interest. Thus, this lack of including light-collection losses explicitly can be treated as an overall constant for a given PVT geometry.

source are shown as solid triangles with drop lines (energies also shown in Table 1), and the energy of the corresponding CEs calculated with Eq. (2) are shown as open triangles with drop lines. Each graph shows the "normal" energy-broadened spectrum and the (unrealistic) 1% energy-broadened spectrum. The usefulness of the 1% energy-broadened spectra is that they clearly show the position and asymmetrical structure of the CM and CE. These features are much less obvious in the "normal" energy-broadened spectra, where the position of the CM is shifted to slightly lower energies than the CE energies for both PVT and NaI(Tl).

One interesting difference between the PVT and NaI(Tl) model distributions is the appearance of X-ray escape peaks. In the photoelectric absorption process, characteristic X-rays are emitted by the absorber atom when the incident gamma ray has an energy greater than or equal to the binding energy for the core electrons in the absorber element, e.g., around 30 keV for iodine in NaI(Tl). In the majority of cases, however, this X-ray is reabsorbed near the original interaction site, if the interaction occurs near the surface of the detector, the X-ray may escape, thus lowering the total energy deposited in the detector by the amount equal to the X-ray photon energy. These escape peaks are seen in the simulations discussed here for NaI(Tl), but not for PVT since the resolution is not sufficient to reveal these features.

As can be seen in the upper graph of Fig. 4, the NaI(Tl) pulse-height spectrum for ^{133}Ba is dominated at high energy by the photopeaks for the two primary gamma rays. The X-ray escape peak for the 384 keV line can also be seen around 320 keV. For PVT (lower graph of Fig. 4), the Compton continuum dominates. For both materials, the CM location cannot be accurately identified by inspection in the "normal" energy-broadened spectrum, but can be clearly seen in the 1% energy-broadened spectrum. In these 1% energy-broadened spectra, the CM can be seen to sit upon the structure resulting from partial energy deposition from multiple Compton events.

For ^{57}Co, the low energy of the two dominant peaks (122 and 136 keV) plus the escape peaks (~90 and ~110 keV) leads to a broad structure in the NaI(Tl) spectrum (upper graph in Fig. 5). However, the contribution to the CM from the lower-energy photopeak (122 keV) can just be resolved. The CMs in PVT (lower graph in Fig. 5) cannot be resolved by inspection. The 1% energy-broadened spectra show the location of the actual CMs.

The presence of high-energy gamma rays from ^{60}Co (Fig. 6) and ^{137}Cs (Fig. 7) make the presence of the photopeaks and the CMs somewhat more easily discerned. For ^{232}Th, the high-energy photopeak can easily be seen in NaI(Tl) (upper graph of Fig. 8), but the CM is somewhat obscured. While the ^{232}Th photopeak cannot be seen in PVT (lower graph of Fig. 8), the CE structure can be seen.

6. Experimental fitting results

Experimental data were obtained for the five radionuclides for analysis of the energy calibration methodology. The NaI(Tl) detector had dimensions of 10×10 cm $\times$ 40.6 mm ($4 \times 4 \times 16$ in.). The PVT detector had dimensions of $3.8 \times 35.6 \times 172.7$ cm ($1.5 \times 14 \times 68$ in.). Multiple data sets were obtained on the detector systems as part of the calibration and operation of the detectors. While these physical detectors are larger than the modeled detectors, the size difference did not affect the results from the application of the calibration method.

To determine the position of the CM and CE energies from the data for NaI(Tl) and PVT, and the photopeaks for NaI(Tl), a parabola was fit to each of the spectral regions of interest, and the positions of the CMs were found. The spectra in the region of the CM, and, where appropriate, the photopeaks, were fitted to the equation

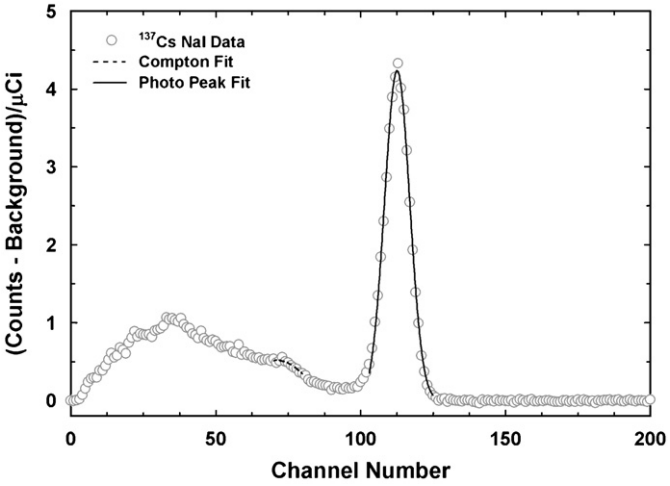

Fig. 9. Example of fitted experimental NaI(Tl) data for the ^{137}Cs photopeak and CE.

$$M = A + B(C_N - C_{N0})^2 \quad (4)$$

where M is the magnitude of the experimental spectrum for an isotope, A and B are fitting constants, C_N is the channel number, and C_{N0} is the channel number at which the maximum in the parabola occurs. For the Compton part of the spectra, this maximum value corresponds to the CM channel, which is not the same as the CE channel. Fig. 9 shows a measured NaI(Tl) spectrum for ^{137}Cs with the fit for both the photopeak and the CE.

For NaI(Tl) experimental data, the photopeak positions were determined for all five radionuclides, but the CM were only found (as described above) for three radionuclides: ^{60}Co (low-energy peak), ^{137}Cs and ^{232}Th. The other two radionuclides (^{57}Co and ^{133}Ba) and the higher energy peak from ^{60}Co could not be included in the analysis because of the complications of interference of other spectral features in the energy region of interest around the CM. Data were measured with the PVT-based scintillator and CMs were found as described above for four radionuclides: ^{60}Co (low-energy peak), ^{133}Ba, ^{137}Cs and ^{232}Th. The other radionuclide (^{57}Co) could not be included in the analysis because of the complications of interference by buildup of down-scattered photons in the low energy region of interest. The results for the fitting parameters of the NaI(Tl) and PVT spectra for the measured radionuclides are shown in Table 2.

The position of the CM is always found at a lower energy than the theoretical energy of the CE calculated from Eq. (2) because of multiple factors, including the physics of the scattering process, multiple scattering events, and imperfections in the scintillator material [7,8,28]. The channel values found for the CM, which can be determined from the fit to the experimental data, thus require a correction factor to relate its value to the energy of the corresponding CE.

This correction from CM channel, which can be found in the experimental spectra, to CE channel, which is not directly observable in the experimental data, is performed by creating a ratio based on data extracted from the MCNP theoretical spectra. The number of counts in the theoretical spectrum at the CE and the number of counts at the CM are found. The ratio for each radionuclide energy and detector type (NaI(Tl) or PVT) is then found from the number of counts at the location of the CE divided by the number of counts at the CM in the theoretical spectra:

$$R_{\text{Theory}} = (\text{Counts at CE})_{\text{Theory}}/(\text{Counts at CM})_{\text{Theory}}. \quad (5)$$

Table 2
Parameter results and errors from the fitting of experimental data from a 512-channel multi-channel analyzer to Eq. (4)

Radioisotope	A	B	C_{N0}	Line or CE energy (keV)
Photo peak in NaI(Tl)				
^{57}Co	15.4(9)[b]	−1.24(172)	20.9(12)	122
^{133}Ba	6.09(7)	−0.242(13)	61.1(1)	356
^{137}Cs	75.7(1)	−8.90(201)	110.1(2)	662
^{60}Co	2.463(1)	−0.0222(19)	198.5(1)	1173
^{60}Co	2.03(1)	−1.980(20)	226(10)	1333
^{232}Th	0.263(4)	$-8.29(74)\times10^{-4}$	447.8(3)	2614
Compton maxima in NaI(Tl)				
^{137}Cs	0.517(19)	−0.00212(85)	71(2)	478
^{60}Co[a]	0.532(71)	$-7.50(150)\times10^{-4}$	148(1)	963
^{232}Th	0.0517(40)	$-3.52(366)\times10^{-4}$	398(4)	2381
Compton maxima in PVT				
^{133}Ba	3.17(3)	−0.0166(47)	19.4(8)	207
^{137}Cs	0.950(12)	$-5.06(69)\times10^{-4}$	55.6(9)	478
^{60}Co[a]	0.831(5)	$-1.92(9)\times10^{-4}$	136(1)	963
^{232}Th	0.059(2)	$-1.05(38)\times10^{-5}$	333(7)	2381

[a] CE for the 1173 keV gamma (963 keV).
[b] The number shown in the ( ) is the one sigma standard deviation in the last reported digit, e.g. 15.4 ± 0.9.

Table 3
Ratios for Compton edge to Compton maxima values

Nuclide	Line energy (keV)	CE energy (keV)	PVT CE-to-CM ratio	NaI(Tl) CE-to-CM ratio
^{133}Ba	356	207	0.75	0.786
^{137}Cs	662	478	0.88	0.688
^{60}Co	1173	963	0.96	0.878
^{232}Th	2614	2381	0.85	0.411

Relevant ratio values resulting from the theoretical spectra in Figs. 4–8 are given in Table 3. This CE-to-CM ratio, as derived from the theoretical spectra, is then used with the results for the parabolic fit to the experimental data (Compton Maximum at C_{N0} in Table 2) to find the channel number at which the same ratio of counts occurs in the experimental data. The expected number of counts at the CE in the experimental data is found from

$$(\text{counts at CE})_{\text{Experiment}} = (\text{counts at CM})_{\text{Experiment}} R_{\text{Theory}}. \quad (6)$$

The channel number above the CM at which this number of counts occurs is the CE location. This derived channel number is then identified as the channel at which the CE energy is found.

This procedure can be used in the field to provide an energy calibration if a spectrum can be obtained. The ratios given in Table 3 determined from the theoretical spectra are different for NaI(Tl) and PVT because of the different response of these detector materials. These listed ratios are potentially model dependent, specifically on the energy broadening used to generate the theoretical spectra. This was tested by further modeling and it was found that the ratio in fact is relatively model independent (varying from 2% to 11% depending on energy) for a reasonable range of PVT detector energy-broadening values (from 14% to 50%). This amounts to about a 10 keV uncertainty from the ratio in the Compton peak energy at 1 MeV, which is small compared to the features of PVT spectra.

Combining the fitting results shown in Table 2 and the energies for the NaI(Tl) photopeaks, a linear relationship between the photopeak energy and channel number is obtained (Fig. 10). In this figure, the least-squares fit straight line is to the channel numbers determined from the fit to the six photopeaks only. The open triangles for the Compton data are the CM positions, and the solid triangles are these values corrected by the method of the CE-to-CM ratio values listed in Table 2 described above. This correction amounts to about 10 channels for the 512-channel data shown here. In all cases, the corrected data lie on the straight line calculated from the photopeak positions. The slope of the line shown in Fig. 10 is 5.826(25)[5] keV/channel, with an energy intercept of 10(6) keV.

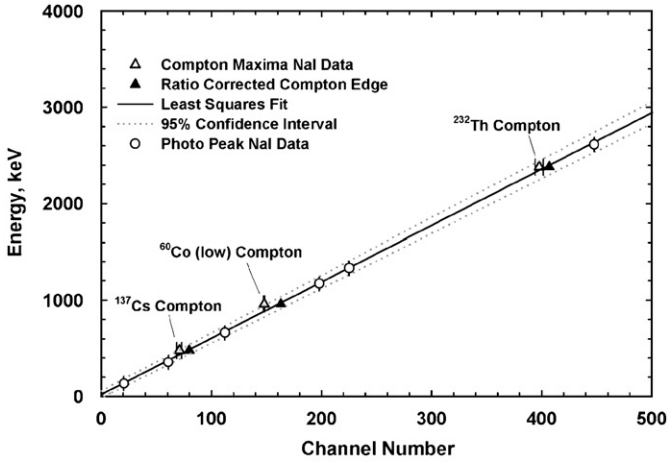

Fig. 10. The linear relationship between experimental NaI(Tl) peak and CE energies and the channel numbers determined with a parabolic fit to the spectral regions of interest for four radionuclides. The data values can be identified through the C_{N0} values in Table 2.

[5] The number shown in ( ) is the one sigma standard deviation in the last reported digit, e.g. 5.826 ± 0.025.

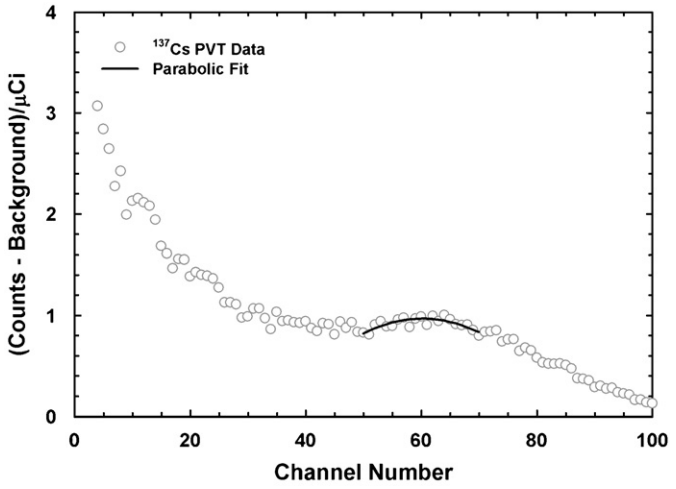

Fig. 11. Results of the least-squares fit of Eq. 4 to the experimental data from PVT for ^{137}Cs over channels 50–70.

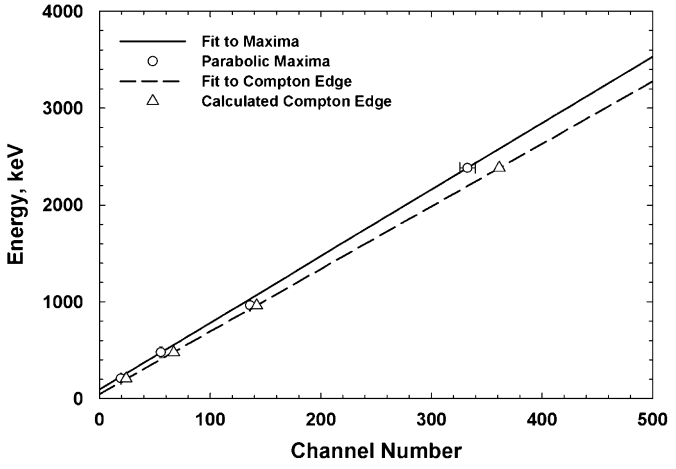

Fig. 12. The linear relationship between experimental PVT CE energies and the channel numbers determined with a parabolic fit to the spectral regions of interest for four radionuclides. The solid line is drawn through the Compton maxima values while the dashed line is through the derived CE values. The data values can be identified through the C_{N0} values in Table 2.

Fig. 11 shows an example of the fit of Eq. (4) to the ^{137}Cs spectrum from the PVT-based detector. For the PVT data, the Compton maximum energies from one ^{60}Co line (1173 keV gamma ray with a CE at 963 keV), ^{133}Ba, ^{137}Cs and ^{232}Th were plotted against channel numbers obtained from the parabolic fits to the data, and a straight line was fit to the data from three isotopes (solid line in Fig. 12). From the CM values, the location of the actual CE was calculated as described above for the CE-to-CM ratio values listed in Table 2. The corrected CM (triangles) positions are plotted in Fig. 12, with a straight line fit (dashed line in Fig. 12). The slope of the dashed line shown in Fig. 12 is 6.454(15) keV/channel, with an energy intercept of 47(3) keV. The linearity is excellent, but the two lines have different slopes, with the dashed line representing the correct energy versus channel calibration. This change in slope demonstrates the importance of the calculated CE-to-CM corrected positions in the calibration of the scintillator in order to get the true energy as a function of channel number. This energy calibration approach has also been applied to another independent data set for a different PVT detector geometry with equal success.

Thus, the linearity of the experimental results implies that calibration of PVT-based scintillators, for at least the detector configurations described in this paper, can be achieved by use of only two[6] isotopes each giving one datum point, such as ^{137}Cs and ^{232}Th, ignoring any non-linear effects.

7. Conclusions

It has been shown that some configurations of PVT scintillators can be energy calibrated with two isotopes from a least-squares fit of a parabola to the observed Compton Maxima, and a prescribed ratio correction of these data to obtain the position (channel number) of the Compton Edge. With this method, it has been demonstrated with NaI(Tl) data that the Compton Edge can be located on average to about ± 1 channel, which corresponds to about ± 6 keV for the particular set of experimental data used, and for PVT to about ± 5 channels, which corresponds to about ± 33 keV.

The CE calibration methodology was used on NaI(Tl) to verify the accuracy of the results since NaI(Tl) can also be calibrated with traditional methods for the full-energy peaks. Excellent agreement was obtained between the full-energy calibration method compared and the CE methodology, thus validating the application of this calibration method to PVT. This method can now be applied to energy calibration of fielded PVT detectors for Energy Windowing applications using two selected gamma-ray sources, which was the goal of the study.

Acknowledgements

This work was supported by the United States Department of Homeland Security. Pacific Northwest National Laboratory is operated for the United States Department of Energy by Battelle under contract DE-AC05-76RLO 1830. PNNL-SA-56684/PIET-43741-TM-681.

References

[1] R.T. Kouzes, Public protection from nuclear, chemical, and biological terrorism, in: A. Brodsky, R.H. Johnson Jr. (Eds.), The 2004 Health Physics Society Summer School, Medical Physics Publishing, Madison, WI, 2004 (Chapter 3).
[2] R.T. Kouzes, Am. Sci. 93 (2005) 422.
[3] J.H. Ely, R.T. Kouzes, J.E. Schweppe, E.R. Siciliano, D. Strachen, D.R. Weier, Nucl. Instr. and Meth. A 560 (2006) 373.
[4] MCNP X-5 Monte Carlo Team, MCNP—A General Purpose Monte Carlo N-Particle Transport Code, Version 5, LA-UR-03-1987, Los Alamos National Laboratory, April 2003. The MCNP code can be obtained from the Radiation Safety Information Computational Center (RSICC), P. O. Box 2008, Oak Ridge, TN, 37831–6362.
[5] C. Can, X-Ray Spectrometry 32 (2003) 280.
[6] L.K. Herold, R.T. Kouzes, Trans. Nucl. Sci. NS-38 (1991) 231.
[7] BG Lowe, Nucl. Instr. and Meth. A 439 (2000) 247.
[8] A. Sood, R.P. Gardner, Nucl. Instr. and Meth. B 213 (2004) 100.
[9] J.C. Vitorelli, A.X. Silva, V.R. Crispim, E.S. da Fonseca, W.W. Pereira, Appl. Radiat. Isot. 62 (2005) 619.
[10] E. Yilmaz, R. Pekoz, C. Can, X-Ray Spectrom. 35 (2006) 42.
[11] S. Normand, B. Mouanda, S. Haan, M. Louvel, IEEE Trans. Nucl. Sci. NS-49 (4) (2002) 1603.
[12] S. Avdic, S.A. Pozzi, V. Protopopescu, Nucl. Instr. and Meth. A 565 (2006) 742.
[13] L.G. Chiang, R.B. Oberer, Method to correlate CFD discriminator level and energy deposition by neutrons and photons in a fast plastic scintillating detector, Oak Ridge National Laboratory Report ORNL/TM-2000/193, Oak Ridge National Laboratory, Oak Ridge, TN.
[14] M. Marseguerra, E. Padovani, SA Pozzi, Prog. Nucl. Energy 43 (2003) 305.

[6] A zero offset in the data is possible, thus requiring two experimental data points and not just one. The zero offset is usually small and thus only a small error would be introduced if just a single isotopic line was used for PVT energy calibration.

[15] M. Marseguerra, Padovani, S.A. Pozzi, M. Da Ros, Nucl. Instr. and Meth. B 213 (2004) 289.
[16] J.A. Mullens, J.S. Neal, P.A. Hausladen, S.A. Pozzi, J.T. Mihalczo, Nucl. Instr. and Meth. B 241 (2005) 804.
[17] E. Padovani, P. Peerani, M. Da Ros, SA Pozzi, Nucl. Instr. and Meth. A 557 (2006) 599.
[18] I. Pázsit, SA Pozzi, Nucl. Instr. Meth. A 555 (2005) 340.
[19] S.A. Pozzi, R.B. Oberer, L.G. Chiang, J.K. Mattingly, J.T. Mihalczo, Nucl. Instr. and Meth. A 481 (2002) 739.
[20] S.A. Pozzi, J. Segovia, Nucl. Instr. and Meth. A 491 (2002) 326.
[21] S.A. Pozzi, E. Padovani, M. Marseguerra, Nucl. Instr. and Meth. A 513 (2003) 550.
[22] S.A. Pozzi, J.A. Mullens, J.T. Mihalczo, Nucl. Instr. and Meth. A 524 (2004) 92.
[23] S.A. Pozzi, R.B. Oberer, J.S. Neal, IEEE Trans. Nucl. Sci. NS-52 (2005) 3141.
[24] S.A. Pozzi, I. Pazsit, Nucl. Sci. Eng. 153 (2006) 60.
[25] E.R. Siciliano, J.H. Ely, R.T. Kouzes, B.D. Milbrath, J.E. Schweppe, D.C. Stromswold, Nucl. Instr. and Meth. A 550 (2005) 647.
[26] XCOM Photon Cross Sections Database, National Institute of Standards and Technology, Washington, DC, 2006. 〈http://physics.nist.gov/PhysRefData/Xcom/html/xcom1.html〉
[27] R.B. Firestone, in: VS Shirley (Ed.), Table of Isotopes, eighth ed., Wiley, New York, 1996.
[28] N. Kudomi, Nucl. Instr. and Meth. A 430 (1999) 96.